Correspondence

Simulation, Manufacturing, and Evaluation of a Sonar for a Miniaturized Submersible Explorer

Jonas Jonsson, Erik Edqvist, Henrik Kratz, Monica Almqvist, and Greger Thornell

***Abstract*—Single-beam side-scan sonar elements, to be fitted on a miniaturized submersible, are here simulated, manufactured, and evaluated. Finite element analysis simulations are compared with measurements, and an overall observation is that the agreement between simulations and measurements deviates from the measured values of 1.5 to 2°, for the narrow lobe angle, by less than 10% for most models. An overall finding is that the lobe width along the track direction can be accurately simulated and, hence, the resolution of the sonars can be predicted. This paper presents, to the authors' knowledge, the world's smallest side-scan sonars.**

I. Introduction

Subglacial lakes are attracting increasing scientific interest. Many are believed to have been isolated by thick ice layers for tens of thousands of years and contain hydrothermal vents which could provide conditions suitable for life to flourish independently of the world outside. The largest of these, Lake Vostok in Antarctica, is the size of Lake Ontario and is covered by an ice sheet up to 4 km thick [1].

The Miniature Autonomous Submersible Explorer (MASE) [2] is a vehicle proposed to investigate the limitations of miniaturization of an instrumented submersible designed for astrobiology-related exploration in places such as subglacial lakes on Earth and the ice-covered Jovian moon Europa. A similar vehicle with subsystems for environmental research in small and harsh environments on Earth is the Deeper Access, Deeper Understanding (DADU) submersible, measuring only 20 cm in length and 5 cm in diameter, but retaining a high functionality enabled through the use of microelectromechanical systems (MEMS) [3].

On DADU, a side-scan sonar [4] is to be used for navigation and mapping, and hence as a complement to the camera system. As a design tool, as well as for the understanding of heavily miniaturized sonars, the set-up and verification of computer based models are important. In this paper, miniaturized single-beam sonar elements are modeled using COMSOL Multiphysics (version 3.5a, COMSOL AB, Stockholm, Sweden), a finite element analysis (FEA) software, and the results compared with first-order approximations and measurements on manufactured sonars.

In [5], a limited investigation of such a sonar beam was made. However, only lower frequencies and 2-D geometries were employed. Also, there were no comparisons with first-order approximations or experimental results, and the beam shape was not studied. Another example, using ATILA to simulate a 2-D sonar transducer [6] also lacks comparison with experimental results. Comparisons between FEA and measurements on live sonars have been performed using software other than COMSOL Multiphysics [7], but only for the transducer's short axis, which is of less importance for the side-scan sonar application. Several finite element methods, boundary element methods, and combinations thereof exist for sonar applications [8]–[10]. However, no thorough evaluation of the coupled physical problem of 3-D acoustics and 3-D piezoelectrics for high-frequency sonars has been found with comparisons to manufactured sonars.

The scientific objective of this study is to explore to what degree, and with what advantages and disadvantages, heavily miniaturized sonar elements can be described and modeled with increasing sophistication, whereas the more technical goal is to build and characterize what, to the authors' knowledge, is the world's smallest side-scan sonar.

II. Sonar Element Design

The width of the main lobe, determined by the lateral size of the element and the sound wavelength, sets the image resolution in the horizontal direction [11]. To compare different sonars, the half-width at half-maximum (HWHM) angle is useful. An approximation of this angle can be found through the beam pattern function, $b(\theta)$,

$$b(\theta) = 20\log\left|\frac{\sin v}{v}\right|, \quad v = \frac{1}{2}kL\sin\Theta, \tag{1}$$

where $k = 2\pi/\lambda$ and L is the length of the transducer [12].

The DADU vehicle requires small and lightweight elements. A trade-off between the dimensions and the operational frequency of the sonar was made, and from this the sonar elements were designed to be 50 mm long, 1.5 to 2 mm wide, and to have an operating frequency in the order of 500 to 700 kHz. For field-tests, sonar electronics for an operational frequency of 666 kHz were acquired from DeepVision AB, Linköping, Sweden. The transducer material chosen was lead zirconate titanate (PZT) ceramic

Manuscript received May 20, 2009; accepted October 21, 2009. This work was supported by MISTRA—The foundation for strategic environmental research, Sweden.

J. Jonsson, E. Edqvist, H. Kratz, and G. Thornell are with the Ångström Space Technology Centre, Ångström Laboratory, Uppsala University, Uppsala, Sweden (e-mail: jonas.jonsson@angstrom.uu.se).

M. Almqvist is with the Department of Measurement Technology and Industrial Electrical Engineering, Lund University, Lund, Sweden.

Digital Object Identifier 10.1109/TUFFC.2010.1429

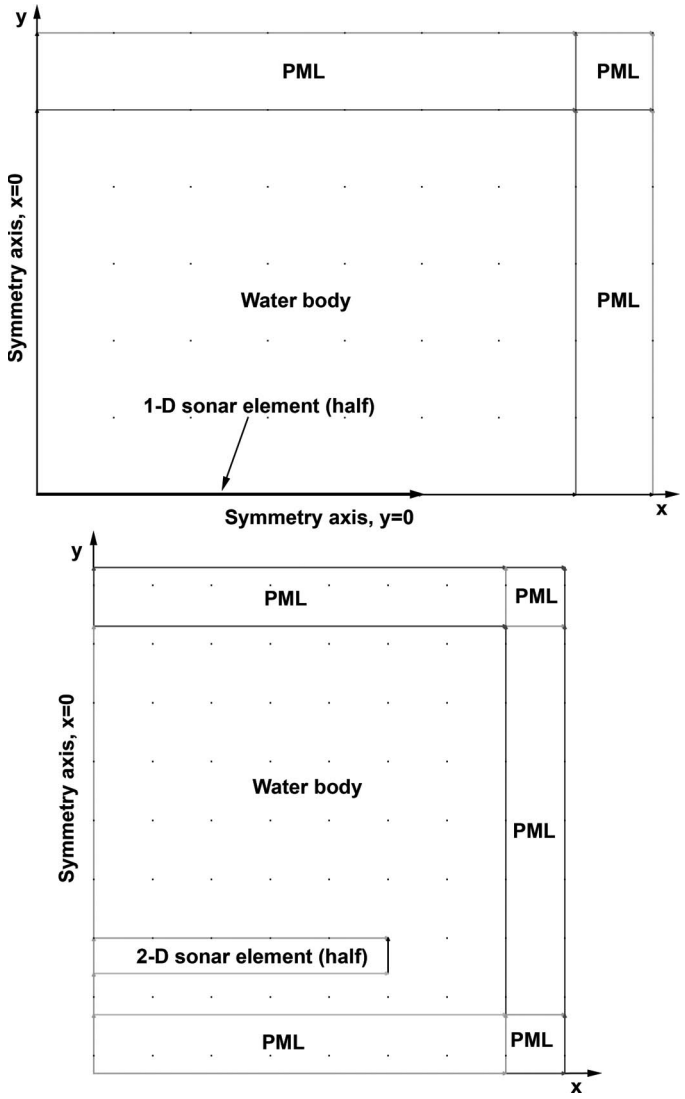

Fig. 1. Model A (top) and Model B (bottom) of the long axis of Sonar 1.

plates, 3 mm thick with Ag electrodes (PKI-402, Piezo Kinetics Inc., Bellefonte, PA) and 2 mm thick with AgPd electrodes (PIC 151, PI Ceramic GmbH, Karlsruhe, Germany).

III. Simulations

COMSOL Multiphysics was used to simulate the behavior of these sonars. The Acoustics Module was used to analyze 4 different models, labeled A–D, for both the long and short axis of the sonars. For the simpler models, where a line, Model A, or surface, Model C, with preset pressure amplitude represents the transducer, only the acoustics part was used. When using the material properties for the PZT, such as in model B and D, the multiphysics interaction was set to fluid-elastic [13].

For all models, the water body sub-domains were set with the software's pre-defined material properties functions. Perfectly matched layers (PMLs) set to the Cartesian type and the appropriate absorbing directions, were used.

A meshing density corresponding to 12 degrees of freedom per wavelength was used for all models [13]. Simplifications allowed by symmetry were made when possible. The beam shapes were calculated and plotted for a distance from the sonar elements equal to that employed for the measurements. From this data the HWHM angles were extracted.

A. Model A: 2-D Mode With 1-D Sonar Element

The simplest model contains a single line, representing the sonar element, transmitting into a rectangular body of water with a symmetry axis at $x = 0$ and $y = 0$, see Fig. 1(top). For the long axis of the sonar element, a 25-mm line is used, labeled 1-D sonar element (half) in Fig. 1(top). For the model of the short axis, this line is 0.75 mm for Sonars 1 through 3, and 1 mm for Sonar 4. Extending from this, a rectangle labeled Water body represents the water into which the acoustic signal is transmitted.

A pressure amplitude of 10 Pa was set as a boundary condition for the transducer line. A far-field variable of full integral type [13] was defined on this line to permit calculation of the beam shape. The boundaries along the x- and y-axis, excluding the 1-D sonar element, were set to sound-hard boundary (wall), whereas the outer boundaries of the PMLs were set to radiation condition.

B. Model B: 2-D Mode With 2-D Sonar Element

Whereas Model A used a preset pressure amplitude, this model uses fluid-elastic coupling. To include the actual PZT material used in the sonars, a 2-D representation of the element was used for the sonar with a thickness of 3 or 2 mm, depending on the material, see Fig. 1(bottom). A time-harmonic electrical potential of 10 V was applied to the top of the element and the bottom was grounded. The left vertical line was set to symmetry.

C. Model C: 3-D Mode With 2-D Sonar Element

In the first 3-D model, a surface element was set to transmit an acoustic pressure with an amplitude of 10 Pa into a 3-D body of water, similarly to Model A, see Fig. 2(top).

Using symmetry planes (normal to the x-, y- and z-axis), only one-fourth of the sonar element needs to be modeled. The element is thus 25 mm long and either 0.75 or 1 mm wide, Table I, and the other settings are the same as for the 2-D mode counterpart, Model A.

D. Model D: 3-D Mode With 3-D Sonar Element

The final model is a complete 3-D model, with a 3-D PZT element radiating into a 3-D water body, Fig. 2 (bottom). Symmetry surfaces are here employed along the x- and y-axis in the model. As in Model B, the thickness of

TABLE I. SONAR DESIGN AND MEASUREMENT PARAMETERS.

Sonar element	Material	Length/ width (mm)	Frequency used for length/width (kHz)	Thickness (mm)	Tungsten/epoxy matching layer (wt-%)	Long axis distance (mm)	Short axis distance (mm)
1	PKI-402	50/1.5	500/500	3.0	none	352.7	35.1
2	PKI-402	50/1.5	495/495	3.0	80/20	354.9	36.2
3	PKI-402	50/1.5	462/666	3.0	72/28	354.9	25.3
4	PIC 151	50/2.0	531/666	2.0	72/28	354.9	135.7

the PZT element is also considered here. Surrounding the element is a 0.75-mm-thick water body, and outside of this, 0.75-mm-thick PMLs. As in Model B, a potential of 10 V was applied to the top electrode.

IV. PHYSICAL EXPERIMENTS

A. Manufacturing

The PZT plates were cut into 50-mm-long by 1.5- or 2-mm-wide pieces, Table I, using semiconductor dicing equipment and a diamond blade. Strips of 66 μm thick copper foil were attached to the electrode layers on the top and the bottom with a conductive adhesive.

A matching layer (ML) [14] with a thickness of one quarter of a wavelength at the frequency 666 kHz, was applied to 3 of the sonars. Generally, a composite is used [15]–[17] to get the right acoustical impedance. Here a mixture of tungsten powder and epoxy resin was used, Table I. The elements were placed in open brass boxes with an SMB connector.

The elements were aligned and centered to the opening of the brass box, and a mixture of epoxy resin and finely grained cork (16:1 by weight) was packed around them to act as an acoustically light backing.

B. Measurements

Hydrophone measurements were conducted to investigate the beam shapes of the sonars using a needle hydrophone (S/N 084, Precision Acoustics Ltd, Dorset, UK). The system consisted of a preamplifier, a hydrophone booster amplifier, a digital oscilloscope, a 300-L watertank, a positioning system with 4 stepping motors, a signal generator, and a computer with control software. The hydrophone in combination with the amplifiers used, offered a sensitivity in the order of 19.4 μV/Pa.

For each of the sonars, the operational frequency was determined through a frequency scan from which the peak response was noted. Each element was characterized at different distances in steps of 1 mm, with a step resolution of 10 μm, along the 2 axis of the element. Bursts of 10 cycles with an amplitude of 10 V at the determined frequency for each sonar element and at a fixed frequency of 666 kHz were used. In all experiments, the distance between the hydrophone and the sonar element was calculated from the measured pulse time and the speed of sound (1482 m/s), Table I.

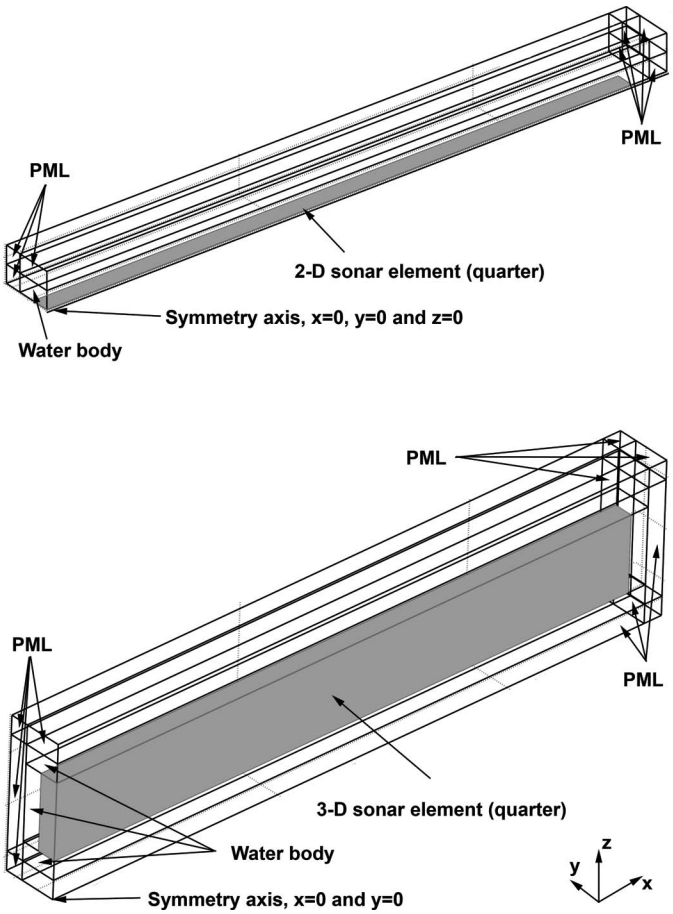

Fig. 2. Model C (top) and Model D (bottom) of Sonar 1.

C. Imaging Tests

Two imaging tests were performed, a bench test and a field test. In both cases Sonar 2 was used.

The bench test was performed in a 1.2 × 1.2 × 0.5 m water tank. Using a stepper motor, the sonar was swept at a speed of 1.2 cm/s in front of 2 solid metal spheres, 7.5 cm in diameter and spaced 20 cm center-to-center apart. The spheres were suspended in the water using fine strings, 45 cm from the sonar path.

The field test was performed in a lake from a boat traveling at a speed of about 0.5 m/s.

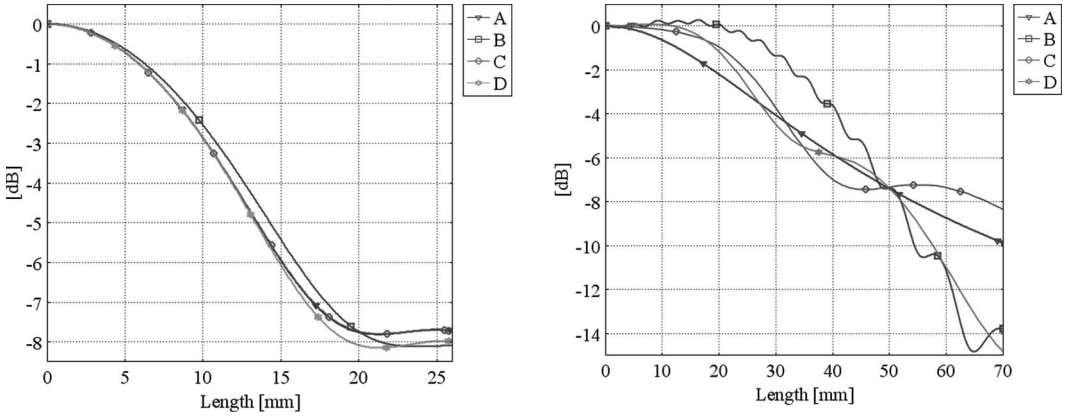

Fig. 3. Beam shape results from modeling showing the relative sound pressure level for Models A–D for the long side (left) and the short side (right) of Sonar 1.

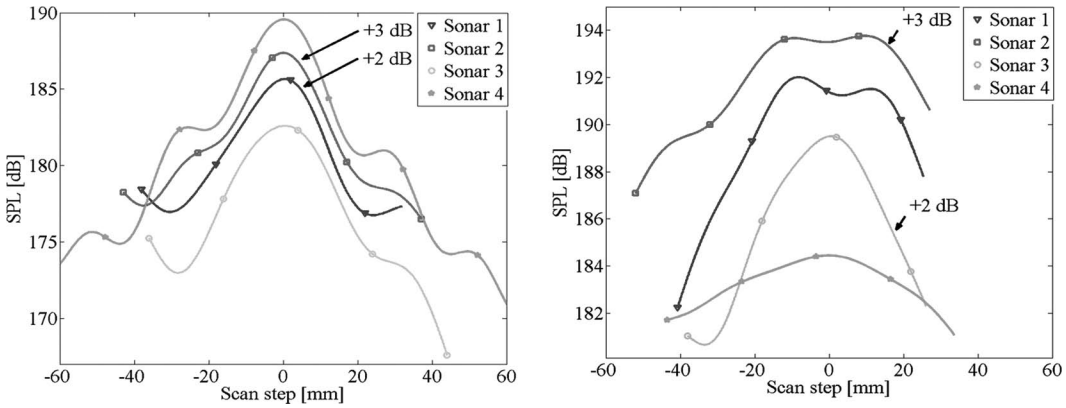

Fig. 4. Sound pressure level along the long axis of Sonars 1–4 (left). The graphs of Sonar 1 and Sonar 2 have been shifted by +2 and +3 dB, respectively, for clarity. The sound pressure level along the short axis of Sonars 1–4 (right). The graphs of Sonar 2 and Sonar 3 have been shifted by +3 and +2 dB, respectively, for clarity. (Note that Sonar 4 was measured at a larger distance than the others in this graph.) Only every 20th data point has been marked.

TABLE II. COLLECTION OF THE RESULTS OF THE HWHM ANGLES.*

			HWHM angles (degrees)							
Sonar element	Size (mm)	Frequency (kHz)	Beam pattern function	Comsol Model A	Comsol Model B	Comsol Model C	Comsol Model D	Measured left	Measured right	Average of meas.
1	50	500	1.50	1.66	1.77	1.66	1.66	1.79	1.56	1.68
	1.5	500	60.9	34.7	46.7	38.2	36.2	33.9	34.4	34.2
2	50	495	1.52	1.68	1.78	1.68	1.68	1.55	1.52	1.54
	1.5	495	61.9	34.8	46.2	37.0	34.8	N/A	38.5	38.5
3	50	462	1.63	1.76	1.89	1.76	1.78	2.00	1.89	1.95
	1.5	666	41.0	30.2	39.7	30.0	33.4	32.8	30.0	31.4
4	50	531	1.41	1.58	1.86	1.59	1.60	1.53	1.47	1.50
	2.0	666	29.5	24.9	24.1	21.5	19.6	N/A	13.2	13.2

*Left and right refer to the side of the main lobe from which the values were extracted.

V. RESULTS

To calculate the beam pattern approximated HWHM angles in Table II, Eq. (1) was used.

The results from calculating and plotting the beam shapes for the relative sound pressure levels (SPLs) along the long and short axis of Models A–D are shown for Sonar 1 in Fig. 3. From this, and similarly for the other sonar elements, the HWHM beam angles were extracted.

The computational power required varied significantly. The complex Model D required over 52 GB of working memory, whereas the memory requirement was just about 1 GB using Model A for the same sonar.

For each sonar, the data obtained from both beam shape measurements were plotted. A low-pass Butterworth filter was applied to the raw data, see Fig. 4. The HWHM beam widths in Table II were calculated from the filtered data.

The resulting image from the bench test can be seen in Fig. 5. The sonar was swept to the far left in the image,

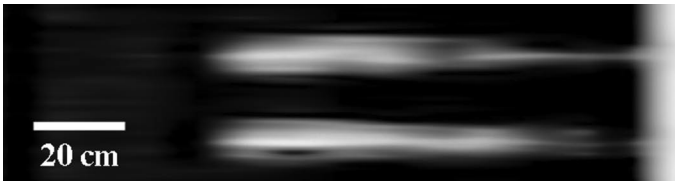

Fig. 5. Sonar image of bench test of 2 metal spheres in an aquarium.

at a distance of 45 cm. To the far right, the aquarium wall can be seen.

A portion of the data acquired from the field test using Sonar 3 can be seen in Fig. 6. Along this stretch, the sonar traveled top-down along what corresponds to the left side of the image, marked as 0 on the scale. The shore line can be seen along the right edge, at 10 to 15 m distance on the scale. In between, several rocks of different sizes are imaged.

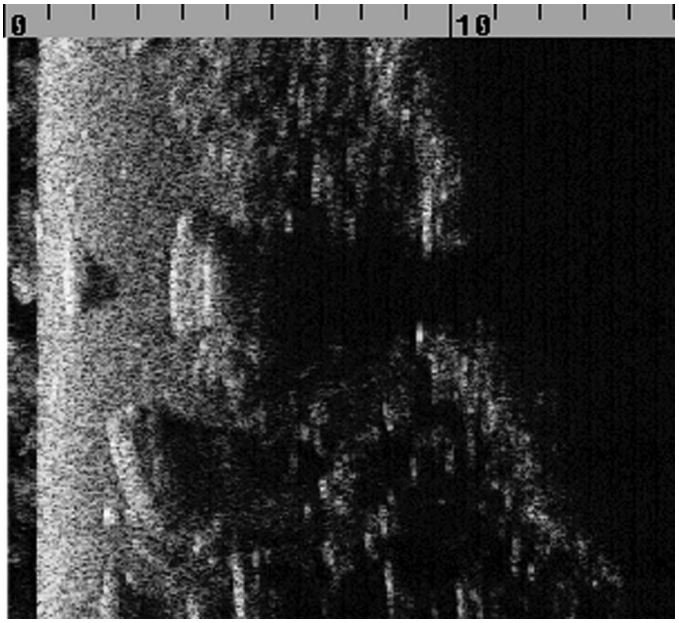

Fig. 6. Sonar image of the bottom of a lake, 10 to 15 m from the shoreline. The scale is in meters.

VI. Discussion

Working miniaturized sonars for small vehicles such as the DADU submersible have been successfully built and tested. From Table II, it can be seen that the first-order approximation deviation from the physical results for the long axis ranges from almost 1% (Sonar 2) to over 16% (Sonar 3). For the short axis, the deviation is much larger, ranging from 30% to over 120%. Thus, the beam pattern approximation does not agree well with the measurements when the wavelength is close to the considered dimension of the element.

On comparing the results of the simulations (see Table II) it can be seen that for the long axis, Model A, C, and D give very similar results, differing by at most 1 and 2% (Sonars 3 and 4), whereas Model B deviates from the other three by as much as 17% (Sonar 4). From this observation alone, it is therefore believed that Models A, C, and D give a more correct result than Model B for the long axis. Also for the short axis, Model B deviates much from the others, about 20%, except for the case with Sonar 4, where all models deviate more from each other, with at most 27% between Model A and D. The short axis result of Model B, Fig. 3 (right), gives a jagged response in its beam shape compared with the others. A preliminary investigation indicates that the jaggedness derives from the interference of waves emanating from the end of the transducer in the model, because the inclusion of a well-placed absorber inside the water domain resulted in a smoother curve.

Comparing the simulation results with those from the measurements, an overall observation is that the modeling is quite accurate, but mostly for the long axis lobe angle where it deviates most for Model B, with 16% for Sonar 2 and 24% for Sonar 4. The others deviate by less than 10%. Regarding the short axis, it can be seen that Model B deviates significantly from the measurements, between 20% and 83%, compared with the other models. The discrepancies for the other models are below 12%, and often 6% or less, with the exception of the extremes of Sonar 4, ranging from 49% to 89%.

Comparing the models, it can be seen that Model B stands out from the others, with a larger deviation, when compared with the measurements. Comparing the sonars, Sonar 4 showed the largest deviations from the measured values on the short axis.

Taking this into consideration, the best overall agreement with the measurements on the sonars, with a deviation less than 10% (except for the short axis of Sonar 4) is provided by Models A and D. However, with the main interest here being accurate determination of only the HWHM angle of the long axis, and when taking into consideration the complexity of the models and the computational power required to solve them, Model A, with a simple 1-D sonar element in a 2-D water body, appears more attractive. Comparing Fig. 1(top) and Fig. 2(bottom), the computational power requirement can also be further decreased for Model A, if needed, by reducing the size of the water domain.

The sonar geometries modeled here are simple. With a verified model, future studies could involve more complex sonar geometries, and investigate the effect of the matching- and backing layers, and edge effects from the brass box walls and the element itself, on the acoustic beam shape. These effects are not readily described analytically, but could be studied with multiphysics models, and result in even better agreement between models and manufactured sonars.

Both the bench and field tests demonstrated a well-working sonar system, although the imaged objects were somewhat smeared. In the bench test, the smearing is in the beam direction, Fig. 5, and found to be within the time

frame where echoes and scatterings from the confined test environment contributed to the signal response.

In the field test, Fig. 6, the rocks are elongated a bit in the travel direction because of the difficulty to operate the boat at a constant speed and direction. The turbulence from the boat is the source of the noise seen within the first meter.

All in all, the tested sonars performed very well for the intended application.

VII. Conclusion

This paper presents the manufacturing, testing, and modeling of, to the authors' knowledge, the world's smallest side-scan sonars. It was found that the HWHM angle of the main lobe in the along-track direction can be accurately simulated using COMSOL Multiphysics, even with the less-elaborate approach examined. Hence, the resolution of the sonars can be predicted. The sonar was found to perform well during field tests, in which the environment was imaged with good quality and range.

Acknowledgments

The authors would like to acknowledge the support from and helpful discussions with S. Hultqvist, L. Andersson at COMSOL, F. Elmgren at DeepVision AB, and T. Stepinski and J.-Å. Schweitz at Uppsala University.

References

[1] A. P. Kapitsa, J. K. Ridley, G. D. Robin, M. J. Siegert, and I. A. Zotikov, "A large deep freshwater lake beneath the ice of central East Antarctica," *Nature*, vol. 381, pp. 684–686, Jun. 20, 1996.

[2] F. C. Bruhn, F. D. Carsey, J. Köhler, M. Mowlem, C. R. German, and A. E. Behar, "MEMS enablement and analysis of the miniature autonomous submersible explorer," *IEEE J. Oceanic Eng.*, vol. 30, pp. 165–178, 2005.

[3] H. Nguyen, J. Jonsson, E. Edqvist, J. Sundqvist, H. Kratz, and G. Thornell, "A heavily miniaturized submersible—A terrestrial kick-off," presented at 10th ESA Workshop on Advanced Space Technologies for Robotics and Automation, Noordwijk, The Netherlands, 2008.

[4] A. P. Cracknell and L. Hayes, *Introduction to Remote Sensing*. New York: Taylor & Francis, 1991.

[5] G. McRobbie, P. Marin-Franch, and S. Cochrane, "Beam characteristics of ultrasonic transducers for underwater marine use," presented at COMSOL User Conf., Birmingham, UK, 2006.

[6] H. Meestouri, A. Loussert, and G. Keryer, "Simulation of sonar transducer by two-dimensional finite element method, ATILA code and GiD graphical interface," in *Oceans 2008—MTS/IEEE Kobe Techno-Ocean*, pp. 1190–1196.

[7] R. Lerch, "Finite element analysis of piezoelectric transducers," in *Proc. IEEE Ultrsonics Symp.*, 1988, pp. 643–654.

[8] D. J. W. Hardie and A. B. Gallaher, "Review of numerical methods for predicting sonar array performance," *IEE Proc. Radar Sonar Navig.*, vol. 143, pp. 196–203, Jun. 1996.

[9] A. Gallaher, P. Macey, and D. Hardie, "Numerical optimization of sonar arrays using FE/BE methods," *Oceans'98—Conf. Proc.*, 1998, pp. 395–398.

[10] S. S. Jarng, "Comparison of barrel-stave sonar transducer simulations between a coupled FE-BEM and ATILA," *IEEE Sens. J.*, vol. 3, pp. 439–446, Aug. 2003.

[11] W. H. Key, "Side scan sonar technology," in *Oceans 2000 MTS/IEEE Conf. Exhibition*, Providence, RI, pp. 1029–1033.

[12] L. E. Kinsler, A. R. Frey, A. B. Coppens, and J. V. Sanders, *Fundamentals of Acoustics*. New York: Wiley, 2000.

[13] *COMSOL Acoustics Module User's Guide*, version 3.5a. COMSOL AB, Stockholm, Sweden, 2007.

[14] D. Callens, C. Bruneel, and J. Assaad, "Matching ultrasonic transducer using two matching layers where one of them is glue," *NDT Int.*, vol. 37, pp. 591–596, 2004.

[15] S. Lees, R. S. Gilmore, and P. R. Kranz, "Acoustic properties of tungsten-vinyl composites," *IEEE Trans. Sonics Ultrason.*, vol. 20, pp. 1–2, 1973.

[16] R. F. Vogel, "Transducers with screen printed matching layers," in *IEEE Ultrasonics Symp.*, New York, NY, 1985, pp. 704–709.

[17] Y. S. Yoon, S. H. Kim, S.-J. Lee, H. K. Kim, and M.-J. Lee, "Fabrication and frequency response of dual-element ultrasonic transducer using PZT-5A thick film," *Sens. Actuators A*, vol. 125, pp. 463–470, 2006.